The electronic structure of the metastable layer compound $1T - CrSe_2$

1997 J. Phys.: Condens. Matter 9 10173

(http://iopscience.iop.org/0953-8984/9/46/015)

J. Phys.: Condens. Matter **9** (1997) 10173–10184. Printed in the UK PII: S0953-8984(97)81910-8

The electronic structure of the metastable layer compound 1T-$CrSe_2$

C M Fang, C F van Bruggen, R A de Groot, G A Wiegers and C Haas

Chemical Physics, Materials Science Centre, University of Groningen, Nijenborgh 4, 9747 AG Groningen, The Netherlands

Received 17 February 1997

Abstract. The electronic structure of the metastable compound 1T-$CrSe_2$ ($a = 3.399$ Å, $c = 5.911$ Å, space group $P\bar{3}m1$) was calculated with and without spin polarization using the LSW method. The energy is 0.29 eV/mol $CrSe_2$ lower for the spin-polarized calculation. The total magnetic moment of $+2.44\ \mu_B$ on Cr consists of $3.28\ \mu_B$ in spin-up and $0.84\ \mu_B$ in spin-down states; the total number of 3d electrons on Cr is 4.12, much greater than expected for Cr(IV) $3d^2$. The Cr 3d-based bands overlap the selenium 4p-based valence band which implies strong covalency of the Cr–Se bonding. At the Fermi level there are electrons and holes with Cr 3d character, and holes with Se 4p character. The results clearly indicate the reduction of the cations and the presence of holes in the Se 4p valence band. $CrSe_2$ is a magnetic metal. Similar calculations for VSe_2 showed a very small energy difference between the magnetic and non-magnetic states, indicating that VSe_2 is a non-magnetic metal.

1. Introduction

Some of the early transition metal dichalcogenides, viz. VS_2, CrS_2 and $CrSe_2$, do not exist in a stable state. However, they can be obtained as metastable in the $Cd(OH)_2$ type structure (as the stable compounds TiS_2, $TiSe_2$, VSe_2, etc) by topotactic oxidation (deintercalation) at ambient temperature of alkali metal intercalates MTX_2 (M = alkali metal). Murphy *et al* [1] were the first to prepare metastable VS_2 with the $Cd(OH)_2$ structure (1T-VS_2) by the oxidation of $LiVS_2$ with I_2 dissolved in acetonitrile. Deintercalation of MTX_2 consists of diffusion of the alkali metal ions out of the space between TX_2 sandwiches and reaction at the solid–liquid interface; in some cases (not for $LiVS_2$) this process is accompanied by parallel shifts of the TX_2 sandwiches. Transition to the stable state (T_2X_3 and X) does not occur at ambient temperature because of the high activation energy for this process.

Why are VS_2, CrS_2 and $CrSe_2$ not stable? When going to the right of the periodic table the d levels progressively decrease in energy and may enter the sulphur or selenium p valence band. With sulphur and selenium a maximum oxidation state of four is found for Ti, Zr, Hf. In the case of TiS_2 the empty d band lies slightly above the valence band; $TiSe_2$ is a semi-metal. When an empty d level lies below the p valence band, the d level will be filled at the expense of the valence band and holes will appear in the top of the valence band, which means that the cations M^{4+} are reduced and the anions X^{2-} are oxidized. At the same time the overlap of the chalcogen p-based bands with the metal d-based bands implies strong covalency of the bonding. The ionic formula $M^{3+}X^{-}X^{2-}$ may approximately describe the products of the internal redox reaction in the metastable compounds VS_2, CrS_2 and $CrSe_2$. The remarkable behaviour of the unit-cell dimensions in the series 1T-$TiSe_2$,

0953-8984/97/4610173+12$19.50

Table 1. Unit-cell dimensions, c/a, z coordinate of Se, unit-cell volume and the metal–selenium bond lengths of 1T-$TiSe_2$, 1T-VSe_2 and 1T-$CrSe_2$ at 300 K. The space group is $P\bar{3}m1$ (No 164).

	a (Å)	c (Å)	c/a	z	V (Å^3)	M–Se (Å)
$TiSe_2$	3.535	6.004	1.698	0.255 04	64.98	2.538 [16]
VSe_2	3.352	6.104	1.821	0.256 65	59.40	2.465 [14]
$CrSe_2$	3.399	5.911	1.738	0.25	59.14	2.456 [7]

1T-VSe_2, 1T-$CrSe_2$ (table 1) is connected in some way to changes in covalency and redox state. A further reduction of the cations to M^{2+} and oxidation of the anions to X_2^{2-} pairs has occurred for MnS_2 and $MnSe_2$ with pyrite or marcasite structures.

Participation of the d electrons in metal–metal bonding and consequently distortion of the $Cd(OH)_2$ structure is particularly strong for the 4d and 5d transition metal dichalcogenides. 1T-TaS_2 (Ta $5d^1$) shows David-star shaped clusters of 13 Ta atoms [2]. Zig-zag chains of the transition metal atoms are present in β-$MoTe_2$ (Mo $4d^2$) [3]. In TcX_2 (Tc $4d^3$) and ReX_2 (Re $5d^3$) the metal atoms are clustered in diamond chains of four-atom clusters [4]. Participation of the d electrons in metal–metal bonding leads to strong metal–metal bonds for the 4d and 5d compounds and to much weaker bonds for the 3d transition metal compounds; e.g. in 1T-VSe_2 (V $3d^1$) the distortion of the $Cd(OH)_2$ structure occurs at low temperature (110 K and 80 K) with presumably small displacements of the V atoms [5]. 1T-$CrSe_2$ shows a remarkable temperature dependence of the unit-cell dimensions and a transition at about 180 K which may be due to clustering of the metal atoms (see below).

1T-$CrSe_2$ was prepared first by Schwarz [6] by oxidation of $KCrSe_2$ in H_2O or diluted acid. Van Bruggen *et al* [7] prepared 1T-$CrSe_2$ by oxidation of $KCrSe_2$ in an oxygen and water free solution of iodine in acetonitrile. $KCrSe_2$ has the $NaCrSe_2$ structure, $a = 3.80$ Å, $c = 21.19$ Å, space group $R\bar{3}m$ [8]; deintercalation is accompanied by parallel shifts of the $CrSe_2$ sandwiches and stacking faults may therefore be present. 1T-$CrSe_2$ has the $Cd(OH)_2$ structure, $a = 3.399$ Å, $c = 5.911$ Å at 300 K, space group $P\bar{3}m1$ (from powder) [7]. Unit-cell dimensions ranging from 3.38 to 3.41 Å for the a axis and 5.89 to 5.92 Å for c were found by Schwarz [6] for different experimental conditions (obtained as such and heated in vacuum). The thermal behaviour was investigated by van Bruggen *et al* [7]. X-ray powder diffraction showed that on heating the compound irreversibly transforms at about 625 K (DTA) into Cr_2Se_3 and Se. In the temperature range 180–625 K the thermal expansion is negative for the c axis and strongly positive for the a axis; c decreases from 5.95 Å at 180 K to 5.85 Å at 550 K. The c/a ratio is 1.74 at 300 K and 1.76 at 180 K. At about 180 K a reversible transition takes place with a decrease of 1% in c and a small increase in a; the cell volume decreases therefore by about 1%. Small thermal effects of this reversible transition were noticed at 164 and 186 K using DTA. Below 180 K some weak extra reflections are present in the powder pattern; however, these could not be indexed on the basis of a simple (e.g. $a\sqrt{3} \times a\sqrt{3}$) supercell. The origin of the negative thermal expansion of the c parameter and the transition at 180 K is not clear. Van Bruggen *et al* [7] suggest a random clustering of the metal atoms, increasing in the range 550–180 K. This clustering would cause a buckling of the sandwiches and an increase of the c from 500 to 180 K; long-range order of the clustering was assumed to occur below 180 K.

The electronic structure of 1T-$CrSe_2$ has been calculated by Myron [9] using a semi-empirical method in which the exchange potential was adjustable. Yoshida and Motizuki [10] obtained the band structure of 1T-$CrSe_2$ by simply using the band structure of $TiSe_2$ and taking into account only the different number of 3d electrons. In both calculations

spin polarization was not included, and the calculations were semi-empirical and not self-consistent. An *ab initio* band structure calculation of 1T-VSe_2 and the effect of the change in the c/a ratio at constant a and the sandwich height parameter z (coordinate of Se) was published by Zunger and Freeman [11].

In this paper we report *ab initio* band structure calculations of 1T-$CrSe_2$ with and without magnetic spin arrangements using the LSW method. The results are compared with similar calculations for 1T-VSe_2 and with the previous calculations for 1T-$TiSe_2$, 1T-VSe_2 and 1T-$CrSe_2$.

2. Band structure calculations

Ab initio band structure calculations were performed with the localized spherical wave (LSW) [12] method using a scalar-relativistic Hamiltonian. We used local-density exchange–correlation potentials [13] inside space-filling, and therefore overlapping, Wigner–Seitz spheres around the atomic constituents. The self-consistent calculations were carried out including all core electrons. The unit-cell dimensions of $CrSe_2$ were those at 300 K found by van Bruggen *et al* [7] and given in table 1; the z parameter of Se was given the value 0.25. An empty sphere was put at the octahedral site in the van der Waals gap (0, 0, 0.5). Similar calculations were performed for 1T-VSe_2. Unit-cell dimensions and the z parameter of Se were those from [7, 14] (table 1). Iterations were performed with $\boldsymbol{k}$ points distributed uniformly in the irreducible part of the first Brillouin zone (BZ), corresponding to a volume of the BZ per $\boldsymbol{k}$ point of the order of 5×10^{-5} Å^{-3}. Self-consistently was assumed when the changes in the local partial charges in each atomic sphere decreased to the order of 10^{-5}.

In the construction of the LSW basis [12, 15], the spherical waves were augmented by solutions of the scalar-relativistic radial equations indicated by the atomic-like symbols 4s, 4p and 3d corresponding to the valence levels of the parent elements V, Cr and Se. The internal l summation used to augment a Hankel function at surrounding atoms was extended to $l = 3$, resulting in the use of 4f orbitals for V, Cr and Se. When the crystal is not very densely packed, as is the case of the layered compounds $CrSe_2$ and VSe_2, it is necessary to include empty spheres in the calculations. The functions 1s and 2p, and 3d as an extension were used for the empty spheres.

3. Electronic structure of $CrSe_2$ and VSe_2

The electronic structure of $CrSe_2$ was calculated with and without spin polarization. From table 2, which lists the input parameters and calculation results (electronic configuration, variational energy and magnetic moment per Cr) it is seen that the variational energy is lower for the ferromagnetic than for the non-magnetic state by 0.29 eV per mol $CrSe_2$. This indicates that $CrSe_2$ is a magnetic compound with local magnetic moments at the Cr atoms. Calculations performed for different magnetic ordering show that an intralayer antiferromagnetic and interlayer antiferromagnetic coupling type of ordering has the lowest energy (about 40 meV lower than the ferromagnetic state). This antiferromagnetic ordering is described in an $a \times a\sqrt{3} \times 2c$ unit cell. Cr moments at (0, 0, 0) and ($\frac{1}{2}$, $\frac{1}{2}$, 0) as well as those at (0, 0, $\frac{1}{2}$) and ($\frac{1}{2}$, $\frac{1}{2}$, $\frac{1}{2}$) are in opposite directions. Cr moments at (0, 0, 0) and (0, 0, $\frac{1}{2}$) are in opposite directions. Other more complicated antiferromagnetic structures are discussed in section 5. The influence of the magnetic ordering on the electronic structure, i.e. on the density of states and the dispersion of the energy bands, is small. We therefore only report

Table 2. Input parameters and results for the non-magnetic and magnetic band structure calculation of $CrSe_2$. R_{WS} represents the Wigner–Seitz radii.

Atom	x	y	z	R_{WS} (Å)	Electronic configuration
Non-magnetic calculation for $CrSe_2$					
Cr 1a	0	0	0	1.1877	$[Ar]4s^{0.22}4p^{0.25}3d^{4.12}4f^{0.02}$
Se 2d	1/3	2/3	0.25	1.7532	$[Ar]4s^{1.93}4p^{4.11}4d^{0.35}4f^{0.13}$
V_a 1b	0	0	0.5	1.1877	$1s^{0.12}2p^{0.15}3d^{0.08}$
Variational energy $= -11\,804.918\,391$ Ryd					
Magnetic calculation for $CrSe_2$					
Cr 1a	0	0	0	1.1877	$[Ar]4s^{0.12}4p^{0.13}3d^{3.28}4f^{0.01}$ (up)
					$[Ar]4s^{0.10}4p^{0.12}3d^{0.84}4f^{0.01}$ (down)
Se 2d	1/3	2/3	0.25	1.7532	$[Ar]4s^{0.96}4p^{1.96}4d^{0.18}4f^{0.08}$ (up)
					$[Ar]4s^{0.96}4p^{2.20}4d^{0.13}4f^{0.04}$ (down)
V_a 1b	0	0	0.5	1.1877	$1s^{0.12}2p^{0.15}3d^{0.07}$ (up + down)
Total moment $= 2.1695\ \mu_B$					
Variational energy $= -11\,804.939\,477$ Ryd					

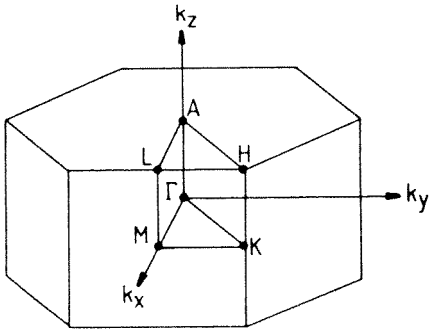

Figure 1. Brillouin zone and high-symmetry points for 1T-$CrSe_2$ and 1T-VSe_2.

the electronic structure of the ferromagnetic $CrSe_2$. The total electronic configuration (spin up + spin down) was found to be the same for the magnetic and the non-magnetic state. The magnetic moments in the ferromagnetic state are Cr $= +2.44\ \mu_B$, Se $= -0.15\ \mu_B$ (mainly in 4p), $V_a = 0\ \mu_B$. The moment on Cr consists of $3.28\ \mu_B$ in spin-up and $0.84\ \mu_B$ in spin-down electrons. The total number of 3d electrons on Cr is 4.12, far from 2 as expected for Cr(IV) $3d^2$. The charges on the atoms and vacancy are Cr $= +1.39$, Se $= -0.52$ and $V_a = -0.35$. Not too much attention should be paid to these charges since they depend on the choice of the Wigner–Seitz radii. Calculations with and without spin polarization were performed for 1T-$CrSe_2$ for slightly different unit-cell parameters, e.g. with the same a, but c increased by 3%; with the same c, but a increased by 3%; with the same a and c, but with $z = 0.24$ or $z = 0.26$. The calculations show small changes of the electronic structure, but in all cases the ferromagnetic state is more stable than the non-magnetic state.

The Brillouin zone (BZ) of 1T-$CrSe_2$ is shown in figure 1, the density of states (DOS) of ferromagnetic $CrSe_2$ in figure 2. The energy bands are shown in figure 3(a) for spin-up and in figure 3b for spin-down states. Table 3 lists the eigenvectors, symmetry and the dominant orbital character at Γ in the BZ.

The two Se 4s states (valence band 2, VB2) are clearly separated from the valence band (VB1), consisting of Se 4p states, by a gap of about 6.5 eV for both spin-up and spin-down

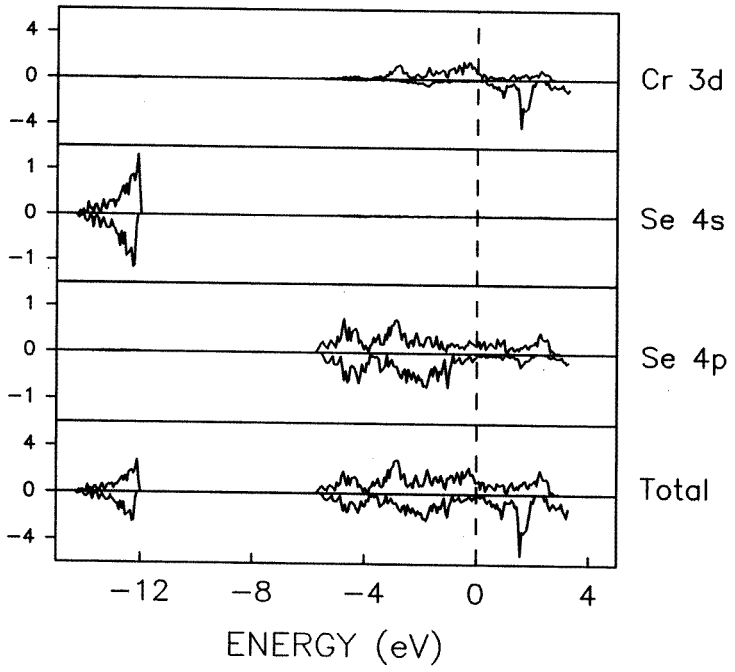

Figure 2. Partial and total density of states (in states/eV) of ferromagnetic 1T-$CrSe_2$. The positive and negative parts represent the density for spin-up and spin-down electrons respectively. The Fermi level is at zero energy.

Table 3. Energies, symmetry and dominant orbital character (OC) at point Γ for the spin-polarized calculations of ferromagnetic 1T-$CrSe_2$, and for non-magnetic 1T-VSe_2. 3d* represents $3d_{xz}$, $3d_{yz}$, $3d_{xy}$, $3d_{x^2-y^2}$.

1T-$CrSe_2$ (spin up)			1T-$CrSe_2$ (spin down)			1T-VSe_2		
E (eV)	Symm.	OC	*E* (eV)	Symm.	OC	*E* (eV)	Symm.	OC
−14.26	1^+	Se 4s	−14.35	1^+	Se 4s	−14.36	1^+	Se 4s
−12.76	2^-	Se 4s	−12.90	2^-	Se 4s	−13.06	2^-	Se 4s
−5.78	1^+	Se $4p_z$	−5.62	1^+	Se $4p_z$	−5.75	1^+	Se $4p_z$
−2.84	3^+	Se $4p_x$, p_y	−1.74	3^+	Se $4p_x$, p_y	−2.05	3^+	Se $4p_x$, p_y
−1.31	3^+	Cr 3d*	+0.37	2^-	Se $4p_z$	−0.33	1^+	V $3d_{z^2}$
−1.13	1^+	Cr $3d_{z^2}$	+0.74	1^+	Cr $3d_{z^2}$	−0.15	3^+	V 3d*
+0.51	2^-	Se $4p_z$	+0.75	3^+	Cr 3d*	+0.01	2^-	Se $4p_z$
+1.12	3^-	Se $4p_x$, p_y	+0.97	3^-	Se $4p_x$, p_y	+1.11	3^-	Se $4p_x$, p_y
+2.61	3^+	Cr 3d	+3.47	3^+	Cr 3d*	+3.02	3^+	V 3d*

states. One of the two Se 4s bands (1^+) is bonding, the other (2^-) antibonding. Both states are occupied, therefore they do not contribute to the net bonding in $CrSe_2$.

The Se $4p_z$ band (1^+) for spin-up electrons is slightly lower than for spin-down because it is pushed down by the stronger hybridization with Cr $3d_{z^2}$; Cr $3d_{z^2}$ (1^+) for spin-up electrons is closer in energy so that the hybridization is larger. The splitting of the Se $4p_z$ bands (1^+ and 2^-) is large: 6.29 eV for spin-up and 5.99 eV for spin-down electrons at Γ; they show also a large and different dispersion along the Γ–A direction. The splitting of Se $4p_z$ at Γ is due to the inter- and intra-layer interactions. The energies of the Se $4p_z$ states which are bonding (Γ_1^+) and antibonding (A_1^+) with respect to the Se $4p_z$–Se $4p_z$ interlayer

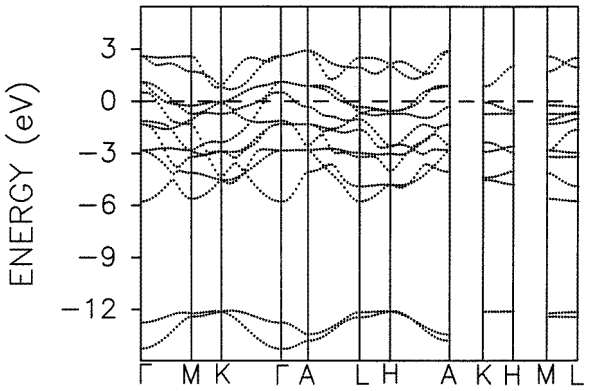

(a)

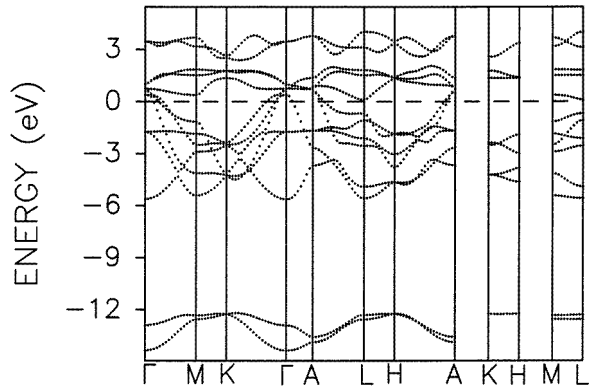

(b)

Figure 3. Dispersion of the energy bands for (a) spin-up and (b) spin-down electrons for ferromagnetic $CrSe_2$.

interactions are

$$E(\Gamma_1^+) = E_0 - \Delta_{\text{interlayer}} - \Delta_{\text{intralayer}}$$
$$E(A_1^+) = E_0 + \Delta_{\text{interlayer}} - \Delta_{\text{intralayer}}$$

With $E(\Gamma_1^+) = -5.78$ eV for spin-up and -5.62 eV for spin-down electrons and $E(A_1^+) = -4.06$ eV for spin-up and -3.67 eV for spin-down electrons, one finds the interlayer interaction energy $\Delta_{\text{interlayer}} = 0.86$ eV and 0.98 eV for spin-up and spin-down electrons, respectively.

The antibonding Se $4p_x$, $4p_y$ (3^-) bands are nearly the same for spin up and spin down, indicating only a slight hybridization with Cr $3d_{xz}$, $3d_{yz}$, $3d_{xy}$, $3d_{x^2-y^2}$. For the bonding Se $4p_x$, $4p_y$ (3^+) bands there is a large difference for spin up and spin down due to a large hybridization with Cr $3d_{xz}$, $3d_{yz}$, $3d_{xy}$, $3d_{x^2-y^2}$ orbitals for spin-up states.

The highest two Cr 3d bands (3^+, mainly $3d_{xz}$, $3d_{yz}$, $3d_{xy}$, $3d_{x^2-y^2}$), corresponding to e_g in an octahedron are nearly separated from the other bands and completely unoccupied for spin-up and spin-down states.

The lower three Cr 3d bands (corresponding to t_{2g} in an octahedron) are unoccupied for spin-down and partly occupied for spin-up states. According to table 2 and figure 3 there

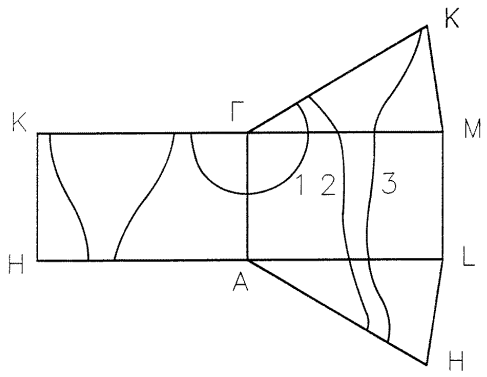

(a)

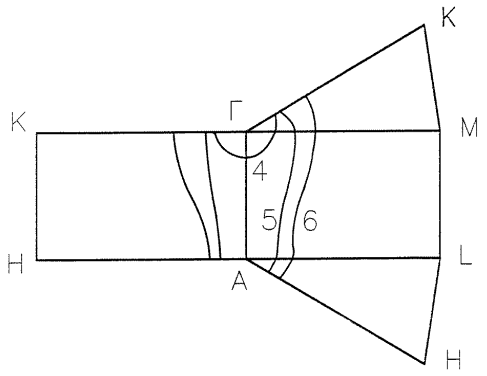

(b)

Figure 4. Fermi surfaces for ferromagnetic $CrSe_2$ (a) spin-up and (b) spin-down states. (1) and (4) are hole surfaces of mixed Cr ($3d_{z^2}$)–Se ($4p_z$) character; (2, 3) and (5, 6) are electron surfaces of mixed Cr (3d*)–Se ($4p_x$, p_y) character.

are also 0.84 Cr 3d spin-down electrons at energies about 2.5 eV below the Fermi energy E_F because of the mixing of Se $4p_x$, $4p_y$ with Cr $3d_{xz}$, $3d_{yz}$, $3d_{xy}$, $3d_{x^2-y^2}$.

The antibonding Se $4p_x$, $4p_y$ band is above E_F at Γ (3^-) for spin-up and spin-down electrons. The same is the case for the Se $4p_z$ band (2^- at Γ). This leads to hole pockets around Γ for spin-up and spin-down states. Holes in the Se 4p band correspond to a reduction of Cr. The formal valence of Cr is lower than Cr(IV); it is more like high-spin Cr(III) or Cr(II), as was also deduced from the total number of 3d electrons on Cr (table 2).

The Fermi surfaces are rather complex as shown in figures 4(a) and 4(b). The Fermi surface for spin-up electrons consists of (1) an ellipsoid around Γ (the charge carriers for this part of the Fermi surface are holes) and (2, 3) two cylinder-like sheets along Γ–A (the charge carriers of these sheets are electrons). The Fermi surface for spin-down electrons consists of (4) an ellipsoid around Γ (the charge carriers for this sheet are holes) and (5, 6) two cylinder-like sheets along Γ–A. The charge carriers (electrons or holes) are in all cases of mixed Cr (3d)–Se (4p) character.

The presence of holes in Se $4p_z$ bands leads to a net covalent intralayer and interlayer bonding between Se atoms, i.e. also bonding across the van der Waals gap. The holes in the Se $4p_x$, $4p_y$ bands cause covalent intralayer bonding between Se atoms.

Band structure calculations for VSe_2 (input parameters and results are given in table 4) for the magnetic and non-magnetic states show a lower energy for the magnetic state; however, the energy difference is only 0.005 eV, and not significant (compare with $CrSe_2$ where the energy difference between magnetic and non-magnetic states was 0.29 eV). The magnetic moment on V in the (ferro) magnetic state is 0.42 μ_B. In order to facilitate comparison of $CrSe_2$ and VSe_2 the dispersion curves of the non-magnetic calculations are given in figures 5 and 6. The calculations of VSe_2 in general agree with those presented by Zunger and Freeman [11], not with those by Myron [9] with respect to the overlap of the metal d- and Se 4p-based bands.

Table 4. Input parameters and results for the band structure calculation of VSe_2.

Atom		x	y	z	R_{WS} (Å)	Electronic configuration
V	1a	0	0	0	1.122	$[Ar]4s^{0.21}4p^{0.26}3d^{3.16}4f^{0.02}$
Se	2d	1/3	2/3	0.256 65	1.754	$[Ar]4s^{1.92}4p^{4.15}4d^{0.32}4f^{0.10}$
V_a	1b	0	0	0.5	1.169	$1s^{0.12}2p^{0.14}3d^{0.07}$

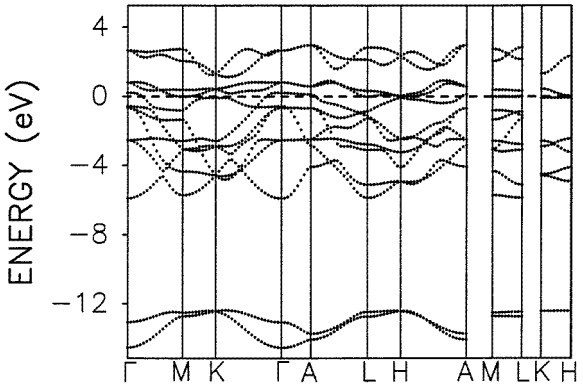

Figure 5. Dispersion of the energy bands for non-magnetic 1T-$CrSe_2$.

4. Comparison of the band structures of $TiSe_2$, VSe_2 and $CrSe_2$

In order to understand the trends for the early transition metal diselenides $TiSe_2$, VSe_2 and $CrSe_2$, we compare the band structures of $TiSe_2$, VSe_2 and $CrSe_2$. Many band structure calculations have been performed for $TiSe_2$. In table 5 we compare our calculations obtained with the LSW method for VSe_2, $CrSe_2$ and $TiSe_2$ [18] with results for $TiSe_2$ and VSe_2, obtained by Zunger and Freeman with the *ab initio* LCAO method [11, 17]. For $TiSe_2$ and VSe_2 our calculations are in general agreement with those by Zunger and Freeman. However, these are some differences. The T nd/X np gaps at the high-symmetry points (Γ, M, L) are smaller (or more negative) in our calculations. In the calculations by Zunger and Freeman only a small number (24) of $\boldsymbol{k}$ points was used to obtain the self-consistent potential, and it is well known that this may lead to appreciable quantitative errors in the calculated energies of the bands, especially near the Fermi level and at the high-symmetry points.

The general pattern of the bands in VSe_2 is qualitatively similar to that previously obtained by us for 1T-$TiSe_2$ [18] (table 5). There are important differences between the

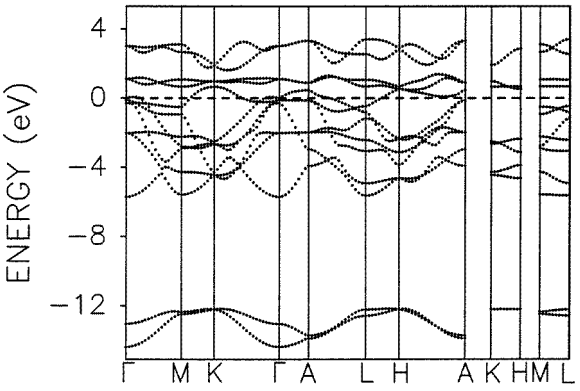

Figure 6. Dispersion of the energy bands for 1T-VSe_2.

Table 5. Comparison of bandwidths and major gaps between the chalcogen p-type and metal d-type bands (denoted by an asterisk) in $TiSe_2$, VSe_2, $CrSe_2$ (non-magnetic state, nm) and $CrSe_2$ (magnetic states, spin up and spin down). Results are given in eV.

Quantity	$TiSe_2$ [17]	$TiSe_2$ [18]	VSe_2 [11]	VSe_2	$CrSe_2$ (nm)	$CrSe_2$ (up)	$CrSe_2$ (down)
Width of VB1	5.70	5.77	5.80	6.86	6.71	6.90	6.59
Width of VB2	2.00	1.86	2.41	2.21	2.17	2.19	2.12
VB1–VB2 gap	6.92	6.78	5.98	6.39	6.41	6.30	6.66
CB1–CB2 splitting (at Γ)	2.1	2.7	1.7	1.9	1.85	2.50	1.49
p–d gaps							
ΓΓ*	0.32	−0.33	0.20	−0.34	−0.78	−1.64	0.46
MM*	2.04	1.32	0.77	0.44	0.49	−0.38	1.49
LL*	1.32	0.41	0.05	−0.33	0.24		
ΓM*	0.12	−0.50	−0.47	−0.62	−1.06		
ΓL*	−0.20	−0.80	−0.71	−0.82	−0.51		
Edge of VB1	Γ_3^-	Γ_3^-	Γ_2^-	Γ_3^-	Γ_3^-	Γ_3^-	Γ_3^-

electronic structures of $TiSe_2$, VSe_2 and $CrSe_2$, due to the different ionicity and the different c/a ratios [11]. The band structure of non-magnetic $CrSe_2$ is approximately the average of the bands for the spin-up and spin-down electrons of the ferromagnetic state. The band width of VB1 for $CrSe_2$ (6.7 eV) and VSe_2 (6.9 eV) is larger than for $TiSe_2$ (5.7 eV), due to the short interatomic distances in $CrSe_2$ and VSe_2 (table 1). The ionicity decreases from $TiSe_2$ to VSe_2 to $CrSe_2$, which causes the increase of the p–d overlap (table 5). However, the bands show some non-systematical behaviour, because of the large c/a ratio for VSe_2 (table 1). A significant difference between the electronic structures of these compounds is that $CrSe_2$ is a magnetic metal and the others are essentially non-magnetic.

5. Electronic structure of $CrSe_2$ and the physical properties

The magnetic susceptibility χ of $CrSe_2$ between 50 and 500 K is about 2×10^{-3} cm^3 mol^{-1}, and shows only a weak dependence on temperature. The weak temperature dependence indicates that $CrSe_2$ is antiferromagnetic, and not ferromagnetic or ferrimagnetic. The magnetic susceptibility of $CrSe_2$ shows at low temperature a paramagnetic tail, presumably

due to a magnetic impurity. Van Bruggen *et al* [7] suggested that this paramagnetic tail is due to the presence of 1.7 mol% $K_{0.5}CrSe_2$ and a paramagnetic contribution from about 2.5 mol% Cr^{4+} ($3d^2$) with spin–orbit coupling, due to self-intercalation of $CrSe_2$ (Frenkel-type disorder). $K_{0.5}CrSe_2$ is antiferromagnetic below 68 K [7]. Below 180 K χ shows two anomalies associated with a phase transition. At high temperature (above 600 K) one observes in χ the effects of the decomposition of $CrSe_2$ into $Cr_2Se_3 + Se$.

With regard to the type of magnetic order of the local magnetic moments on Cr in $CrSe_2$, we remark that the Cr–Cr distance in $CrSe_2$ is very short, i.e. 3.399 Å. The short distances in $CrSe_2$ are (in part) due to the covalent Se–Se bonds, as a result of the presence of holes in the Se (4p) bands. The intralayer exchange interaction J_1 between nearest-neighbour Cr atoms consists of a direct antiferromagnetic interaction J_1' and a ferromagnetic 90° superexchange interaction J_1''. The exchange interaction J_2 between Cr atoms in different layers is expected to be weak and antiferromagnetic. The direct interaction J_1' depends strongly on the Cr–Cr distances: it is large for short Cr–Cr distances. These considerations explain that for compounds with short Cr–Cr distances, the paramagnetic Curie temperature θ is negative, and that for long Cr–Cr distances θ is positive. For example, in $LiCrS_2$ the Cr–Cr distance is 3.464 Å and $\theta = -276$ K [19, 20], and for $NaCrSe_2$ [22] and $KCrSe_2$ [8] the Cr–Cr distances are 3.73 Å and 3.80 Å, and $\theta = +108$ and $+250$ K, respectively. $LiCrS_2$ with a layer stacking as $CrSe_2$ adopts the 120° spin structure; neighbouring layers are coupled antiferromagnetically [20]. More complicated (helical) antiferromagnetic ordering is observed in $NaCrSe_2$ and $AgCrSe_2$ [22]. Figure 7 also shows the relationship between θ and the Cr–Cr distances for $ACrX_2$ compounds (A = Li, Na, K, Ag, Cu; X = S, Se) [8, 19–22]. Because of the very short Cr–Cr distance in $CrSe_2$, we expect strong antiferromagnetic intralayer exchange interactions with $\theta \leqslant -300$ K. As a consequence the magnetic structure will consist of antiferromagnetic layers. For a magnetic structure with ferromagnetic layers with a weak antiferromagnetic coupling between the layers, one would expect a very strong temperature dependence of χ, like that observed for $KCrSe_2$ [8].

Magnetic susceptibility data [23] for VSe_2 show a temperature independent magnetic susceptibility of $\chi = 3 \times 10^{-4}$ cm^3 mol^{-1} (except for a small increase of χ at low temperature, presumably due to paramagnetic impurities). The susceptibility data show that VSe_2 is a non-magnetic compound, without local magnetic moments at V, which is consistent with our band structure calculations.

The small calculated energy difference between the magnetic and non-magnetic states of VSe_2 indicates that it costs very little energy to induce a magnetic moment at the V atoms. This is consistent with the fact that the observed paramagnetic susceptibility of VSe_2 is very large, i.e. there is a large exchange enhancement of the Pauli paramagnetic susceptibility.

Electrical transport (resistivity, Hall effect and thermopower) and magnetic properties were measured by van Bruggen *et al* [7], on powder compacts of $CrSe_2$. The resistivity ρ is 2×10^{-5} Ω m at 300 K and increases to 13×10^{-5} Ω m at 4 K. The transition at 180 K is hardly visible. The Hall coefficient R_H is positive between 300 and 40 K, with a maximum at about 100 K, and becomes negative below 40 K. At 300 K R_H would correspond to 0.5 hole/Cr in a one-carrier model. The thermopower α is positive. A steep rise occurs from 4 to 100 K ($\alpha = +23$ μV K^{-1} at 100 K) and a decrease in the range 100–300 K with a dip at 180 K; at 300 K $\alpha = 10$ μV K^{-1}.

The different sign of the Hall effect and the thermopower at low temperature, and the change of sign of the Hall coefficient with temperature, show that there is mixed electrical conduction in $CrSe_2$, i.e. by electrons and holes. This is consistent with the calculated Fermi surface (figure 4).

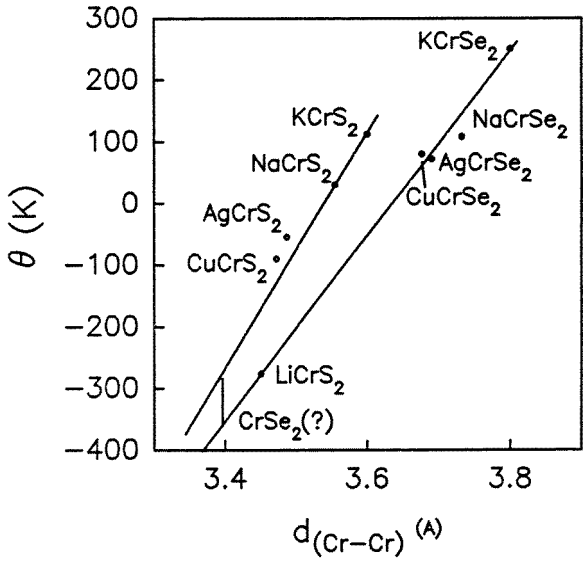

Figure 7. Cr–Cr distances and asymptotic Curie temperature θ for 1T-$CrSe_2$ and some $ACrX_2$ compounds (A = Li, Na, K, Cu, Ag; X = S, Se).

6. Conclusions

Ab initio LSW spin-polarized and non-polarized band structures are calculated for $CrSe_2$ and VSe_2. VSe_2 is non-magnetic while $CrSe_2$ is magnetic; the magnetic moment is about 2.4 μ_B/Cr ion. The valence and conduction bands are formed by the Se 4p and Cr 3d (V 3d) states; the overlap is stronger for the Cr compound. The band structure for the two spin directions of $CrSe_2$ is quite different near the Fermi level. The calculated Fermi surface shows the presence of holes in the Se (4p) bands, and both electrons and holes in the Cr (3d) bands.

Acknowledgment

We thank Henk Bruinenberg for help in the preparation of some figures.

References

[1] Murphy D W, Cross C, DiSalvo F J and Waszczak J V 1977 *Inorg. Chem.* **16** 3027
[2] Brouwer R and Jellinek F 1974 *Mater. Res. Bull.* **9** 827
Wilson J A, Di Salvo F J and Mahajan S 1975 *Adv. Phys.* **24** 117
Spijkerman A, de Boer J L, Meetsma A, Wiegers G A and van Smaalen S *Phys. Rev.* B accepted for publication
[3] Brown B E 1966 *Acta Crystallogr.* **20** 268
[4] Fang C M, Wiegers G A, Haas C and de Groot R A 1997 *J. Phys.: Condens. Matter* **9** 4411
Lamfers H-J, Meetsma A, Wiegers G A and de Boer J L 1996 *J. Alloys Compounds* **241** 4418
[5] van Landuyt J, Wiegers G A and Amelinckx S 1978 *Phys. Status Solidi* a **46** 479
[6] Schwarz H G 1953 *Dissertation* Tubingen
[7] van Bruggen C F, Haange R J, Wiegers G A and de Boer D K G 1980 *Physica* B **99** 166
[8] Tolsma P 1973 *Laboratory of Inorganic Chemistry, Internal Report, University of Groningen*
Fang C M, Tolsma P R, van Bruggen C F, de Groot R A, Wiegers G A and Haas C 1996 *J. Phys.: Condens. Matter* **8** 4381

[9] Myron H W 1981 *Physica* B **105** 120
[10] Yoshida Y and Motizuki K 1982 *J. Phys. Soc. Japan* **51** 2107
[11] Zunger A and Freeman A J 1979 *Phys. Rev.* B **19** 6001
[12] van Leuken H, Lodder A, Czycyk M T, Springelkamp F and de Groot R A 1990 *Phys. Rev.* B **41** 5613
[13] Hedin L and Lundqvist B I 1971 *J. Phys. C: Solid State Phys.* **4** 2064
[14] Rigoult J, Guidi-Morosini C, Tomas A and Molinie P 1982 *Acta Crystallogr.* B **38** 1557
[15] Anderson O K and Jepsen O 1984 *Phys. Rev. Lett.* **53** 2571
[16] Riekel C 1976 *J. Solid State Chem.* **17** 389
[17] Zunger A and Freeman A J 1978 *Phys. Rev.* B **17** 1839
[18] Fang C M, de Groot R A and Haas C, to be published
[19] Bongers P F, van Bruggen C F, Koopstra J, Omloo W P F A M, Wiegers G A and Jellinek F 1968 *J. Phys. Chem. Solids* **29** 977
[20] van Laar B and Ijdo D J W 1971 *J. Solid State Chem.* **3** 590
[21] van Laar B and Engelsman F M R 1971 *J. Solid State Chem.* **6** 384
[22] Engelsman F M R, Wiegers G A, Jellinek F and van Laar B 1973 *J. Solid State Chem.* **6** 574
[23] van Bruggen C F and Haas C 1976 *Solid State Commun.* **20** 251